Biosensors and Bioelectronics 235 (2023) 115409

Contents lists available at ScienceDirect

Biosensors and Bioelectronics

journal homepage: www.elsevier.com/locate/bios

Development of electrochemical Zn^{2+} sensors for rapid voltammetric detection of glucose-stimulated insulin release from pancreatic β-cells

Emma L. Vanderlaan [a,b], James K. Nolan [a,c], Joshua Sexton [a], Carmella Evans-Molina [d,e,f], Hyowon Lee [a,c], Sherry L. Voytik-Harbin [a,g,*]

[a] Weldon School of Biomedical Engineering, College of Engineering, Purdue University, West Lafayette, IN, USA
[b] Indiana Medical Scientist/Engineer Training Program, Indiana University School of Medicine, Indianapolis, IN, USA
[c] Center for Implantable Devices, Birck Nanotechnology Center, Purdue University, West Lafayette, IN, USA
[d] Indiana Center for Diabetes and Metabolic Diseases, Indiana University School of Medicine, Indianapolis, IN, USA
[e] Department of Pediatrics, Indiana University School of Medicine, Indianapolis, IN, USA
[f] Roudebush VA Medical Center, Indianapolis, IN, USA
[g] Department of Basic Medical Sciences, College of Veterinary Medicine, Purdue University, West Lafayette, IN, USA

ARTICLE INFO

Keywords:
Glucose-stimulated insulin secretion
Diabetes
Pancreatic β-cell
Zinc
Electrochemical sensor
Anodic stripping voltammetry

ABSTRACT

Diabetes is a chronic disease characterized by elevated blood glucose levels resulting from absent or ineffective insulin release from pancreatic β-cells. β-cell function is routinely assessed in vitro using static or dynamic glucose-stimulated insulin secretion (GSIS) assays followed by insulin quantification via time-consuming, costly enzyme-linked immunosorbent assays (ELISA). In this study, we developed a highly sensitive electrochemical sensor for zinc (Zn^{2+}), an ion co-released with insulin, as a rapid and low-cost method for measuring dynamic insulin release. Different modifications to glassy carbon electrodes (GCE) were evaluated to develop a sensor that detects physiological Zn^{2+} concentrations while operating within a biological Krebs Ringer Buffer (KRB) medium (pH 7.2). Electrodeposition of bismuth and indium improved Zn^{2+} sensitivity and limit of detection (LOD), and a Nafion coating improved selectivity. Using anodic stripping voltammetry (ASV) with a pre-concentration time of 6 min, we achieved a LOD of 2.3 μg/L over the wide linear range of 2.5–500 μg/L Zn^{2+}. Sensor performance improved with 10-min pre-concentration, resulting in increased sensitivity, lower LOD (0.18 μg/L), and a bilinear response over the range of 0.25–10 μg/L Zn^{2+}. We further characterized the physicochemical properties of the Zn^{2+} sensor using scanning electron microscopy (SEM), cyclic voltammetry (CV), and electrochemical impedance spectroscopy (EIS). Finally, we demonstrated the sensor's capability to measure Zn^{2+} release from glucose-stimulated INS-1 β-cells and primary mouse islets. Our results exhibited a high correlation with secreted insulin and validated the sensor's potential as a rapid alternative to conventional two-step GSIS plus ELISA methods.

1. Introduction

Diabetes, a chronic disease characterized by elevated blood glucose levels, affects more than 37 million people in the United States (Centers for Disease Control and Prevention, 2022). Uncontrolled blood glucose levels result in chronic hyperglycemia, a condition which, over time, causes complications such as chronic kidney disease and peripheral neuropathy (DiMeglio et al., 2018; Nathan et al., 2014). Dysregulation of glucose homeostasis results from either i) an autoimmune attack of insulin-producing β-cells (type 1 diabetes) or ii) peripheral insulin resistance and progressive functional loss of β-cells (type 2 diabetes). Pancreatic β-cells are located in clusters of cells (islets of Langerhans) in the pancreas (Eizirik et al., 2020) (Fig. 1A). Physiologically, β-cells act as the body's glucose sensors, secreting the hormone insulin in response to elevated blood glucose levels. Insulin, in turn, promotes glucose uptake into peripheral tissue cells and maintenance of glucose homeostasis (Fu et al., 2013b) (Fig. 1B). When β-cells lose the capacity to adequately secrete insulin endogenously, the conventional standard of care relies on daily exogenous insulin therapy. Unfortunately, discrete injections fail to adequately replace dynamic glucose control, and despite decades of research, there is still no cure for diabetes (DiMeglio et al., 2018; Pettus et al., 2019). Experimental β-cell replacement therapies aim to restore

* Corresponding author. Weldon School of Biomedical Engineering, College of Engineering, Purdue University, West Lafayette, IN, USA.
E-mail address: harbins@purdue.edu (S.L. Voytik-Harbin).

https://doi.org/10.1016/j.bios.2023.115409
Received 21 February 2023; Received in revised form 12 May 2023; Accepted 17 May 2023
Available online 18 May 2023

physiological glucose-stimulated insulin release by transplanting functional islets or stem cell-derived β-cells into individuals with diabetes. While such approaches have shown some success in Phase 3 clinical trials, remaining challenges have prevented FDA approval (Gamble et al., 2018; Hering et al., 2016; Velazco-Cruz et al., 2019; Witkowski et al., 2021). Thus, an immense amount of translational research continues to focus on functional quality-control measures for replacement β-cell populations in addition to basic mechanistic research targeting diabetes pathophysiology. Assessing β-cell function rapidly and accurately is critical to bringing novel therapies to individuals with diabetes.

The standard method for measuring β-cell function in vitro is the static Glucose-Stimulated Insulin Secretion (GSIS) assay. Static GSIS evaluations involve the following: i) suspending whole islets or β-cells within a physiologic buffer, ii) exposing the cells serially to different glucose concentrations, and iii) later quantifying the amount of insulin secreted using an enzyme-linked immunosorbent assay (ELISA) (Integrated Islet Distribution Program, 2020). ELISAs detect targets of interest (i.e., insulin) by sandwiching the target protein between two antibodies, with one attached to the well-plate and the other attached to a fluorescent molecule. By taking advantage of antibody-antigen binding, ELISAs offer high sensitivity and accuracy but require long incubation times and significant material cost, approximately 2 h and $450 per 96-well plate, respectively. For more advanced β-cell function testing, GSIS may be measured dynamically via perifusion. Dynamic GSIS measurements provide more physiologically relevant information regarding the time-dependent, biphasic response of insulin release through frequent medium sampling (Alcazar and Buchwald, 2019). However, commercial perifusion machines needed to perform dynamic GSIS assays are costly, require extensive training, and still rely on expensive, follow-on insulin detection methods (i.e., ELISA). Recently, microfluidic devices have been explored as alternatives to bulky perifusion machines, most of which also require ELISAs (Adewola et al., 2010; Bauer et al., 2017; Jun et al., 2019; Misun et al., 2020; Patel et al., 2021; Schulze et al., 2021; Xing et al., 2016). Therefore, there is a critical need for an easy-to-use, rapid, and low-cost way of quantifying β-cell function in a continuous, dynamic manner.

Biosensors represent a potential alternative to conventional immunoassays, owing to their ability for rapid target detection and application-specific customization (Akhavan et al., 2012; Bansod et al., 2017; Chen et al., 2013). Furthermore, biosensors may be readily integrated into microfluidic device formats, with the potential to support real-time insulin monitoring without repeated sampling or complex secondary assays (Kratz et al., 2019). To date, several fluorescent insulin biosensors have been reported for quantification of dynamic insulin secretion from β-cells (Dishinger et al., 2009; Glieberman et al., 2019; Lomasney et al., 2013). Although these optical biosensors detect insulin immediately within the microfluidic device, they rely on antibody binding and are limited by the cost of labeling probes, which must be prepared separately and continuously infused downstream of the β-cells (Glieberman et al., 2019). Electrochemical sensors, on the other hand, provide low-cost, highly-sensitive alternatives that can be readily miniaturized for integration into microfluidic devices (Soffe et al., 2019). Although several electrochemical sensors for insulin have been developed for point-of-care applications, they either rely on antibodies for insulin capture (Xu et al., 2013), including sandwich-type voltammetric sensors (Sakthivel et al., 2022), or have a non-specific response susceptible to interference from other molecular species (Martínez-Periñán et al., 2016; Šišoláková et al., 2019).

Although insulin is the active hormone secreted by β-cells in response to elevated glucose levels, several other molecules are co-secreted during granule exocytosis, including C-peptide and zinc (Zn^{2+}) ions (Fig. 1B). In β-cells, Zn^{2+} is highly concentrated in insulin secretory granules by the Zn^{2+} transporter ZnT8, where it acts to stabilize the storage form of insulin at a ratio of 2 Zn^{2+} ions per insulin hexamer (Davidson et al., 2014; Fu et al., 2013b). In previous reports, Zn^{2+} has been targeted as a readily detectable charged species for visualization of

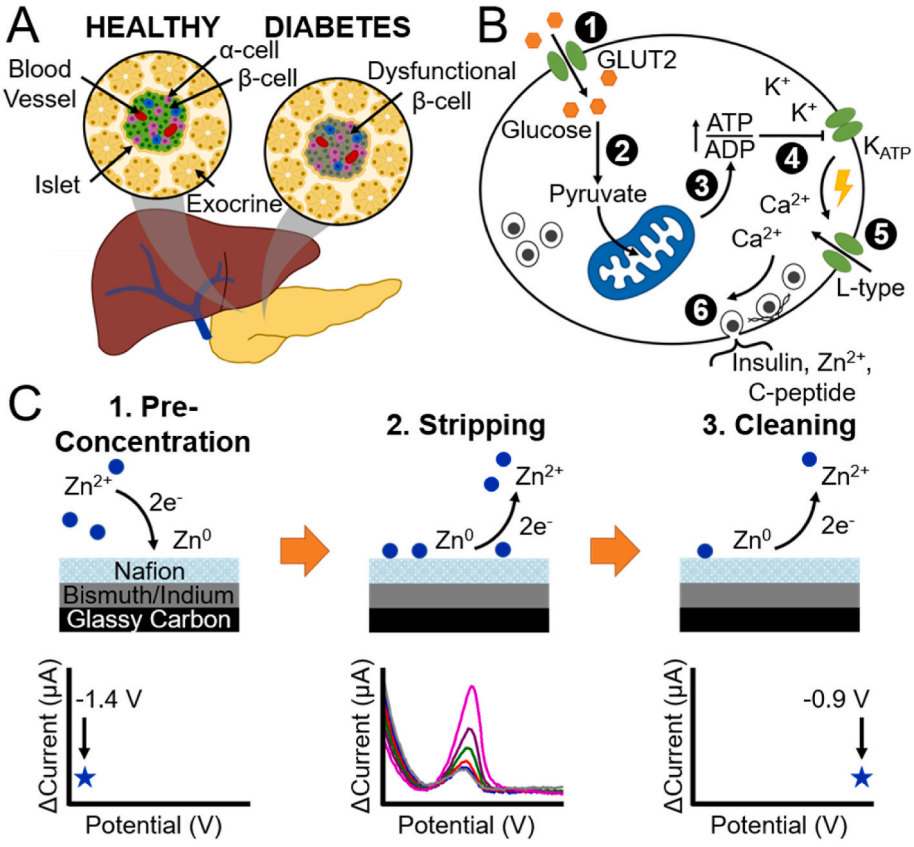

Fig. 1. (A) Pancreatic β-cells may be rendered dysfunctional via type 1 or type 2 diabetes, resulting in little to no endogenous insulin production and the inability to regulate blood glucose levels. (B) Insulin is secreted by β-cells when: 1. Glucose enters via GLUT2 transporters. 2. Glucose is metabolized by glycolysis into pyruvate. 3. The citric acid cycle produces ATP. 4. Increased ATP/ADP levels close K_{ATP} channels and depolarize the cell membrane. 5. Voltage-gated Ca^{2+} channels open, increasing intracellular [Ca^{2+}]. 6. Insulin granules fuse with the plasma membrane, releasing insulin, Zn^{2+}, and other molecules. (C) ASV Protocol: 1. During the preconcentration step, Zn^{2+} ions are reduced onto the surface of the GCE, which is shown modified with layers of Bi/In and Nafion. 2. Zn is oxidized due to the positive-going potential sweep, which generates an electrical current. 3. A cleaning step regenerates the sensor by removing any residual Zn from the electrode.

intracellular insulin secretory granules (Ghazvini Zadeh et al., 2020; Xu et al., 2009) and quantification of spatiotemporal insulin release during GSIS measurements (Qian et al., 2003). The majority of studies implementing this strategy rely on fluorescent Zn^{2+} probes, such as FluoZin-3 (Easley et al., 2009; Qian et al., 2004), ZIGIR (Ghazvini Zadeh et al., 2020), or ZIMIR (Chen et al., 2021; Li et al., 2011). Only one example of an electrochemical method for quantification of Zn^{2+} released from islets has been previously reported, which involved bismuth (Bi)-modified glassy carbon electrodes (GCE) and anodic stripping voltammetry (ASV) (Maghasi et al., 2004). However, sensor characterization was limited, and the sensor was only applied for measurement of stored insulin and Zn^{2+} following complete degranulation from canine pancreatic islets (Maghasi et al., 2004). Islet degranulation, which is induced by exposure to high potassium concentrations, represents a destructive, end-point measurement that does not provide an indication of β-cell function (i.e., glucose-stimulated insulin release). In fact, this process does not occur naturally in vivo, even under pathological conditions (Henquin, 2021). In general, for the ASV technique, voltammetric sensors are used to detect target analytes (i.e., Zn^{2+}) by applying a voltage potential that oxidizes the target species at the electrode surface, generating electrons and a measurable electric current that correlates with analyte concentration (Fig. 1C). For this approach, selectivity and specificity are achieved through the characteristic redox potential of the target metal ion rather than antigen-antibody binding (Borrill et al., 2019). Due to the high sensitivity achieved, ASV has been widely used for detecting trace metals such as Zn^{2+}, defined as less than 100 parts per million (Brown and Milton, 2005), predominantly in environmental applications (Li et al., 2018). Table 1 provides a partial summary of recently developed electrochemical Zn^{2+} sensors along with their performance specifications and associated applications.

Building off the extensive research conducted to date, the objective of the present study was to design and evaluate a sensor for dynamically measuring Zn^{2+} secreted from pancreatic β-cells as an indirect measure of insulin release under physiologically-relevant conditions, including relevant ranges of glucose concentrations. In-vitro GSIS assays typically evaluate ranges of 2.8–28 mM glucose (Alcazar and Buchwald, 2019) to simulate possible in-vivo blood glucose values (Hasslacher et al., 2014). More specifically, design specifications included the following: (1) sensor operation within the standard biological medium used for GSIS assays, namely Krebs Ringer Buffer (KRB), and (2) measurement of physiological concentration ranges of Zn^{2+}. Although Zn^{2+} detection by ASV is conventionally performed in acetate buffer (0.1–0.2 M; pH 4–5) (Borrill et al., 2019), such conditions are harmful to β-cells and other cell populations, whereas KRB represents a physiological medium containing essential ions and nutrients to promote cell health and function (pH 7.2–7.3). Typical insulin secretion rates in mouse islets range from basal levels of 30–50 pg/islet/min to glucose-stimulated levels of 150–200 pg/islet/min (Dishinger et al., 2009), corresponding to approximately 0.1–0.2 pg/islet/min and 0.5–0.75 pg/islet/min Zn^{2+}, respectively, given each insulin hexamer contains two Zn^{2+} ions (Fu et al., 2013b). In comparison, human islets secrete 2–3 fold less insulin (Alcazar and Buchwald, 2019).

To meet these specifications, we characterized how different surface modifications to GCEs affected Zn^{2+} sensitivity and detection range,

Table 1
Comparison of various electrochemical sensors for Zn^{2+} detection using modified carbon electrodes.

Electrode surface modifications	LOD (μg/L)	Linear range (μg/L)	Sensitivity (nA/[μg/L Zn^{2+}])	Detection method	Detection medium	Application	Reference
			Screen-Printed Carbon Electrode				
Nafion with ex-situ Bi film	50	100–2000	23.8	SWASV	0.1 M NaCl/0.1 M Acetate buffer (pH 4.6)	Human sweat	Kim et al. (2015)
MWCNT/Nafion composite with in-situ Bi film	0.3	0.5–100	13.6	DPASV	0.1 M Acetate buffer (pH 4.0)	Lake water	Fu et al. (2013a)
Tin nanoparticles	0.3	1–30	850	SWASV	0.2 M KBr/0.1 M Acetate buffer (pH 4.5)	Drinking water	Trachioti et al. (2018)
Nafion/ionic liquid/graphene composite with in-situ Bi film	0.09	0.1–100	213.7	SWASV	0.1 M Acetate buffer (pH 4.5)	Drinking water	Chaiyo et al. (2016)
Gold nanoparticles with in-situ Bi film	0.05	1–150	178.5	DPASV	Acetate buffer (pH 4.5)	Lake water	Lu et al. (2017)
			Glassy Carbon Electrode				
Electrochemically reduced graphene oxide	6.5	65.4–4086	2.5	DPASV	0.2 M Acetate buffer (pH 5.0)	N/A	Kudr et al. (2016)
In-situ Bi film	2.68	32.7–327	12.1	SWASV	0.1 M Acetate buffer (pH 4.74)	Multivitamin formulations	Fonseca et al. (2015)
Magnetite/fluorinated MWCNT composite with Nafion	0.78	2.55–2125	55	SWASV	0.1 M Acetate buffer (pH 5.0)	Lake water	Wu et al. (2019)
Activated graphene/Nafion composite with in-situ Bi film	0.57	5–100	730	DPASV	0.1 M Acetate buffer (pH 4.5)	Drinking water	Lee et al. (2015)
Ex-situ Bi/In film	0.52	0–120	298	SWASV	0.1 M Acetate buffer (pH 6.0)	River water	Ouyang et al. (2018)
Electrochemically reduced graphene oxide with in-situ Bi film	0.33	1.3–65	410.5	SWASV	0.1 M Acetate buffer (pH 5.0)	Drinking water	Ren et al. (2018)
Iron oxide/graphene composite with in-situ Bi film	0.11	1–100	1039	DPASV	0.1 M Acetate buffer (pH 4.5)	Drinking water	Lee et al. (2016)
PSS/wrinkled reduced graphene oxide composite	0.11	0.33–47	281.4	DPASV	0.1 M Acetate buffer (pH 5.0)	Seawater	Ma et al. (2020)
Alanine	0.00058	0.65–654	201.4	SWASV	Britton-Robinson buffer (pH 4.0)	Drinking water	Kokab et al. (2019)
Ex-situ Bi film	n.r.	n.r.	n.r.	SWASV	0.15 M Phosphate buffered saline (pH 7.4)	KCl-induced total insulin release	Maghasi et al. (2004)
Ex-situ Bi/In film with Nafion	5.4 ± 3.2	10–100	417.3 ± 124.3	SWASV	0.1 M Acetate buffer (pH 4.3)	N/A	This work
Ex-situ Bi/In film with Nafion	2.3 ± 1.5	2.5–500	44.7 ± 10.8	SWASV	KRB (pH 7.2)	N/A	This work
Ex-situ Bi/In film with Nafion	0.18 ± 0.12	0.25–1 1–10	1022.6 ± 334.4 203.4 ± 32.9	SWASV	KRB (pH 7.2)	Glucose-stimulated insulin secretion	This work

SWASV: Square-wave ASV, DPASV: Differential pulse ASV, MWCNT: Multi-walled carbon nanotubes, n.r.: not reported.

including metallic films (i.e., Bi, indium (In), and Bi/In composites) and charge-selective polymer coatings (i.e., Nafion and poly (sodium 4-styrenesulfonate) (PSS)). An electrode configuration, in turn, was down-selected and further characterized morphologically using scanning electron microscopy (SEM) and electrochemically using cyclic voltammetry (CV) and electrochemical impedance spectroscopy (EIS). Finally, to validate the practical application of this electrochemical sensor for detection of β-cell function specifically in response to glucose, we measured Zn^{2+} secreted from two different β-cell populations, a well-established insulin-producing β-cell line and primary mouse islets, and correlated the results to the amount of insulin released as measured by standard ELISA. In the future, we plan to apply the rapid, cost-effective Zn^{2+} sensor described in this work to detect dynamic, glucose-stimulated insulin/Zn^{2+} release in situ.

2. Materials and methods

2.1. Materials

Standard stock solutions of Zn^{2+} and Bi^{3+} were obtained from Sigma-Aldrich (St. Louis, MO, USA). In^{3+} was purchased in the form of Indium (III) nitrate hydrate (Sigma-Aldrich) and used to create stock solutions in ultrapure water. Nafion was obtained as a 5% solution (Sigma-Aldrich) and diluted to working concentrations with 55% ethanol. A 2.5% stock solution of PSS (M_W ~70,000, Sigma-Aldrich) was made with phosphate-buffered saline (PBS, pH 7.4). Metallic film deposition was performed in 0.1 M sodium acetate buffer (pH 4.5). Unless stated otherwise, all other electrochemical analysis procedures were performed in KRB (pH 7.2–7.3; 25 mM HEPES, 115 mM sodium chloride (NaCl), 24 mM sodium bicarbonate ($NaHCO_3$), 5 mM potassium chloride (KCl), 1 mM magnesium chloride hexahydrate ($MgCl_2$ 6 H_2O), 2.5 mM calcium chloride dihydrate ($CaCl_2$ 2 H_2O), 0.1% bovine serum albumin (BSA)) (Integrated Islet Distribution Program, 2020).

2.2. Instrumentation

All electrochemical analyses were performed on a BioLogic SP-200 potentiostat (Seyssinet-Pariset, France) using a typical 3-electrode cell with a GCE working electrode (3 mm diameter), platinum wire counter electrode, and silver/silver chloride (Ag/AgCl) (3 M NaCl) reference electrode. All electrodes were obtained from BASi (West Lafayette, IN, USA). To visualize surface morphology of modified GCEs, SEM was performed on FEI Quanta 3D and Teneo FEG scanning electron microscopes (FEI Company, Hillsboro, OR, USA) by the Life Science Microscopy Facility at Purdue University. For SEM experiments, a rotating disc GCE tip (BASi) was used to accommodate size constraints inside the electron microscope chamber.

2.3. Electrode surface modification

Prior to any modification steps, GCEs were polished with a 0.05 μm alumina suspension (Buehler, Lake Bluff, IL, USA) on a micropolishing pad, according to manufacturer's protocols (BASi). The metallic film was created using conventional electrodeposition procedures. More specifically, the GCE was immersed in 0.1 M sodium acetate buffer containing 20 mg/L Bi^{3+} and 30 mg/L In^{3+}, and a constant voltage of −1.15 V was applied under stirring conditions (800 rpm) until a total charge of 1.4 μA.h was reached (~1.5 min), unless otherwise indicated. The Bi/In-GCE was then rinsed with deionized water and dried with compressed air before use. For all Nafion coatings, a 2 μL droplet was applied to the GCE surface and allowed to dry at room temperature overnight. For mixed Nafion/PSS coatings, a mass ratio of 5.3 (Nafion: PSS) was used (Jia et al., 2007). For PSS coatings, the GCE was submerged in a 0.2 mM PSS solution and CV was performed from −1.4 to −0.9 V for 10 cycles at 100 mV/s (Ma et al., 2020). Before using modified GCEs for Zn^{2+} detection, electrode surface coatings were stabilized by cycling between −1.4 and −0.9 V at 100 mV/s for 10 cycles in KRB.

2.4. Electrochemical analysis procedure

Square-wave ASV was utilized for detection of Zn^{2+} in KRB. Pilot experiments assisted in identification of specific acquisition parameters applied in this study. A 6-min pre-concentration period was applied at −1.4 V under stirring conditions (800 rpm). The ASV acquisition parameters were as follows: 40 mV pulse height, 10 ms pulse width, 4 mV step height, and 5 s quiescent period. A 1-min cleaning period was applied at −0.9 V with stirring to ensure any residual Zn was removed from the electrode surface before subsequent measurements. Calibration curves were established by plotting the height of the Zn^{2+} stripping peak (i.e., peak Δcurrent at −1.15 V vs. Ag/AgCl) corresponding to a range of Zn^{2+} concentrations (i.e., 5–150 μg/L) and fitting a linear regression. Sensor sensitivity was determined as the slope of the regression line. The limit of detection (LOD) was calculated from the following equation, where $S_{y/x}$ was the standard error of the y-intercept and b was the slope (Shrivastava and Gupta, 2011):

$$LOD = 3.3\, S_{y/x} / b$$

For electrochemical characterization of modified electrodes, CV and EIS were performed in 5 mM potassium ferricyanide/ferrocyanide ($[Fe(CN)_6]^{3-/4-}$) with 1 M KCl supporting electrolyte. CV was performed from −0.6 to 0.8 V for 5 cycles at 50 mV/s. EIS was recorded from 1 MHz to 0.1 Hz. Analysis of all electrochemical procedures was performed with EC-Lab software (V11.21, BioLogic).

2.5. Cell culture

Rat insulinoma cells (INS-1832/13; Sigma-Aldrich) were maintained in RPMI-1640 supplemented with 2 mM L-Glutamine (Gibco, Waltham, MA, USA), 1 mM sodium pyruvate (Gibco), 10 mM HEPES (Sigma-Aldrich), 0.05 mM β-mercaptoethanol (Gibco), 10% fetal bovine serum (FBS; HyClone, Logan, UT, USA), and 1% penicillin/streptomycin/amphotericin B (P/S/F; Gibco). For glucose stimulation experiments, INS-1 cells were seeded in T-75 tissue culture flasks at a density of 40,000–50,000 cells/cm^2 and allowed to reach confluency (400,000–500,000 cells/cm^2).

Mouse islets were isolated from 8-week-old male CD1 mice (Jackson Laboratory, Bar Harbor, ME, USA) by the Islet and Physiology Core (Center for Diabetes and Metabolic Diseases, Indiana University School of Medicine). Islets were hand-picked in groups of 100 or 200 islets and placed in Transwell culture inserts (Corning, Cambridge, MA, USA). Islets were maintained in RPMI-1640 supplemented with 10% FBS and 1% P/S/F and were cultured overnight prior to GSIS experiments.

2.6. GSIS assay procedure

To obtain physiological samples of cell-secreted Zn^{2+} and insulin, β-cells from different sources were stimulated with a series of glucose solutions. For INS-1 cells, low glucose (2.5 mM) KRB was applied for 1 h to prime cells before high glucose (15 mM) KRB was applied for 2 h, according to manufacturer's protocols. Each test sample (8 mL) represented an individual flask of cells (~35 million cells, n = 5). Similarly, mouse islets were exposed to different concentrations of glucose following a standard GSIS assay protocol (Integrated Islet Distribution Program, 2020). Briefly, mouse islets were placed in low glucose (2.8 mM) KRB for 1 h to obtain the basal insulin secretion level. Next, islets were incubated in low (2.8 mM) and high (28 mM) glucose KRB for 1 h each. Each test sample (1.5 mL) represented a group of 100–200 islets taken from two different islet isolation batches (n = 5). After exposure to each glucose level, the supernatant was collected for further analysis. The amounts of secreted insulin and Zn^{2+} were determined in the high

glucose sample and compared to baseline. Zn^{2+} was detected by the ASV protocol described above, with a modification of a 10-min preconcentration time. ASV results were then correlated with insulin concentrations, as determined using a murine insulin ELISA kit (Alpco, Salem, NH, USA), which has a dynamic range of 0.1–150 ng/mL and a LOD of 0.089 ng/mL insulin.

2.7. Statistical analysis

Statistical analyses were performed using JMP Pro, Version 16 software (SAS Institute Inc., Cary, NC, USA). For sensor performance parameters, sensitivity and LOD values were calculated from the linear regression equation as described above and compared using a one-way ANOVA and Tukey-Kramer multiple comparison test. P-values less than 0.05 were considered significant.

3. Results and discussion

3.1. Design and fabrication of Bi and In co-modified GCEs

Since their introduction in 2000, Bi-film electrodes have been widely used for trace metal detection owing to their high reproducibility, wide potential window, and ability to form temporary alloys with other heavy metals (Wang, 2005; Wang et al., 2000). Bi-film electrodes have been routinely created by electrodepositing Bi onto carbon electrodes (e.g., GCE) either prior to (ex situ) or simultaneously with metal detection (in situ) (Švancara et al., 2010). Several electrodeposition parameters, including Bi^{3+} concentration, deposition potential, and deposition time, have been shown to affect the morphology of thin films plated ex situ (Švancara et al., 2005; Wang, 2005). This, in turn, modulated how Zn^{2+} interacts with Bi particles during the pre-concentration step and thus ASV stripping peak heights and electrode performance (Economou, 2005; Švancara et al., 2005). Therefore, optimization of these parameters was critical to generating metallic films compatible with ASV detection (i.e., composed of small, uniform metallic deposits without fully-formed crystals) (Švancara et al., 2010). As a first step, the concentration of Bi^{3+} in the electrodeposition medium (0.1 M Acetate buffer, pH 4.5) was varied in increments of 10 mg/L over a concentration range routinely reported in the literature (Serrano et al., 2013). Of the selected Bi^{3+} concentrations, sensors fabricated with 20 mg/L Bi^{3+} yielded significantly improved responses ($p = 0.0052$, $n = 3$), as shown in Fig. S1A, and thus, were selected for all subsequent sensor fabrication and evaluation experiments.

Additional electrode modifications with secondary metals have been reported to improve sensor sensitivity (Lu et al., 2017; Ouyang et al., 2018). More specifically, In has been shown to improve Bi-film electrode performance by increasing the effective surface area and providing more active sites for Zn^{2+} deposition during the pre-concentration step (Ouyang et al., 2018). Additionally, In has a greater overpotential for the hydrogen evolution reaction (Gudić et al., 2010), which is critical for electrochemical analysis of highly electronegative metals such as Zn. For experiments evaluating Bi/In deposition potential and time, Bi^{3+} and In^{3+} concentrations in a 3:2 mass ratio were used in the deposition medium, representing a composition previously found optimal by Ouyang et al. (2018). When Bi/In deposition potential was varied in the range between the reduction potential of In^{3+} and the hydrogen evolution reaction (−0.87 to −1.15 V), sensor sensitivity and LOD were found to be statistically similar ($n = 3$, Fig. S1B), which was distinct from previous reports. However, the calibration curves may have tempered relationships emerging at single Zn^{2+} concentrations, which were more frequently used for parametrization studies in the literature. Interestingly, the amount of In^{3+} deposited, estimated by the height of the In^{3+} oxidation peak at −0.8 V (Wang et al., 2001), increased with more negative deposition potentials ($p = 0.0092$, Fig. S1C), due to increased overpotential. Based on these findings, a deposition potential of −1.15 V was deemed optimal and used for subsequent experiments. Modulation of deposition time also yielded similar calibration curves with no significant difference in sensitivity or LOD values ($n = 3$, Fig. S1D). Since a deposition time of 1.5 min yielded moderately higher sensitivity, albeit non-significant, this time was selected for follow-on experiments. The electrodeposition conditions determined in these pilot parameterization studies were consistent with ranges reported previously for other Bi-films (Kefala et al., 2003; Kim et al., 2015; Ouyang et al., 2018; Serrano et al., 2013).

Once Bi/In deposition parameters were established, different Bi/In film compositions were created by varying the In^{3+} concentration in the deposition medium relative to Bi^{3+} (i.e., 1:0, 3:2, 1:1, 2:3, 0:1 Bi:In mass ratios, $n = 5$). To determine which Bi/In-GCE configuration would best meet the requirements for detecting Zn^{2+} released from pancreatic β-cells, markers of sensor performance (i.e., sensitivity, LOD, and dynamic range) were compared to the target detection range. Given current experimental conditions (i.e., 100–200 islets, 1.5 mL, 1 h), these ranges were estimated to be 0.45–1.5 μg/L and 2.25–6 μg/L, for basal and stimulated secretion levels, respectively. In general, as shown in Fig. 2, the presence of Bi and/or In films substantially improved sensor performance in comparison to bare GCEs, which exhibited a sensitivity of 38.7 ± 2.9 nA/(μg/L Zn^{2+}), a LOD of 218.0 ± 68.1 μg/L Zn^{2+}, and a detection range that fell well outside the target. GCE modifications containing Bi (1:0, 3:2, 1:1, and 2:3 Bi:In) improved both Zn^{2+} sensitivity and LOD, with average values of 27.7–37.9 nA/(μg/L Zn^{2+}) and 3.5–18.6 μg/L Zn^{2+}, respectively. Such observed benefits of Bi modification are consistent with previous reports and result from low background signal and ability to form temporary alloys with Zn^{2+} during preconcentration (Kefala et al., 2003; Romih et al., 2017; Wang et al., 2000). On the other hand, GCEs modified only with In (0:1 Bi:In) exhibited the lowest sensitivity (5.3 ± 1.7 nA/(μg/L Zn^{2+})) and the worst LOD (37.6 ± 13.4 μg/L Zn^{2+}) of the modified GCEs, which would not be suitable for our application (Fig. 2). Interestingly, Bi and In appeared to have synergistic effects on Zn^{2+} detection, resulting in lower LODs and higher or similar sensitivities when compared to electrodes modified with either Bi or In alone. In particular, the Bi/In-GCE containing the highest concentration of In^{3+} (2:3 Bi:In) yielded a sensitivity of 32.9 ± 10.4 nA/(μg/L Zn^{2+}) and a LOD of 3.5 ± 2.0 μg/L Zn^{2+}, falling within the target application range of 0.45–6 μg/L, and thus, was selected for follow-up experiments.

3.2. Evaluation of charge-selective polymer coatings

Although the Bi/In-GCE sensor met stated requirements of detecting Zn^{2+} in the target concentration range, several charge-selective polymer coatings were explored for the purpose of bringing additional physical protection and stability to the sensor. Since the intended application involved Zn^{2+} detection within biological microenvironments containing proteins and other biomolecules, approaches to protect the electrode surface from non-specific binding were investigated. The aim of these experiments was to define how the addition of a polymer layer affected the LOD, sensitivity, and detection range of the Bi/In-GCE.

Nafion has been shown to act as a perm-selective membrane that allows small cations, such as Zn^{2+}, to reach the electrode surface while preventing adsorption of larger or negatively-charged biomolecules (Chaiyo et al., 2016; Kefala et al., 2004). As summarized in Fig. 3A, decreasing Nafion concentration from 5% to 0.5% significantly improved the LOD from 334.9 ± 59.3 to 8.3 ± 10.2 μg/L Zn^{2+} ($p < 0.0001$, $n = 3$), which was attributed to increased Nafion thickness at 5% slowing electron transfer (Jia et al., 2007). Furthermore, the addition of 0.5% Nafion significantly improved the average sensitivity (64.9–86.2 nA/(μg/L Zn^{2+}), $p = 0.0016$, $n = 3$) compared to the Bi/In-GCE and did not impact the dynamic range (Fig. 3A and B), and therefore was selected for follow-up experiments. Additionally, adjusting the fabrication procedure to deposit the Nafion coating on top of the Bi/In film resulted in moderately decreased variation (standard deviation) between sensors (Fig. 3B).

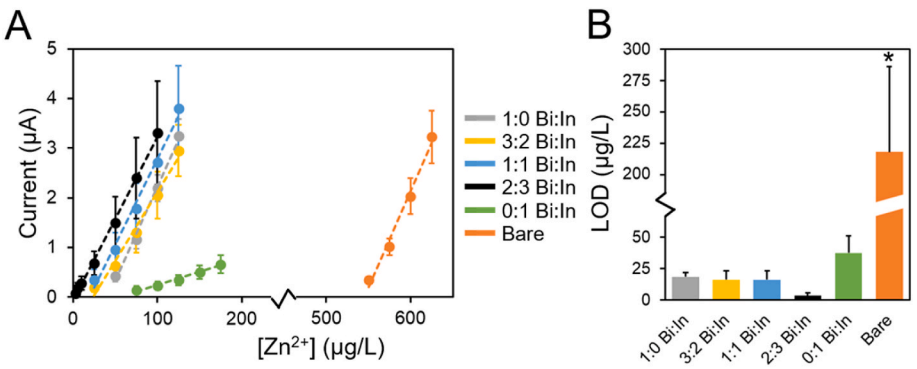

Fig. 2. (A) Calibration curves for Zn^{2+} detection using GCEs modified with different ratios of Bi and In (deposited in 0.1 M Acetate Buffer (pH 4.5) at −1.15 V until −1.4 μA.h cumulative charge) showed substantial improvement in Zn^{2+} detection range when Bi and/or In films are present. (B) Increasing proportions of In^{3+} relative to Bi^{3+} (20 mg/L) in the deposition medium resulted in substantial reduction of LOD for Zn^{2+}. Error bars represent standard deviation (n = 5). * indicates statistically different groups based on one-way ANOVA with Tukey-Kramer multiple comparison test; $p < 0.05$.

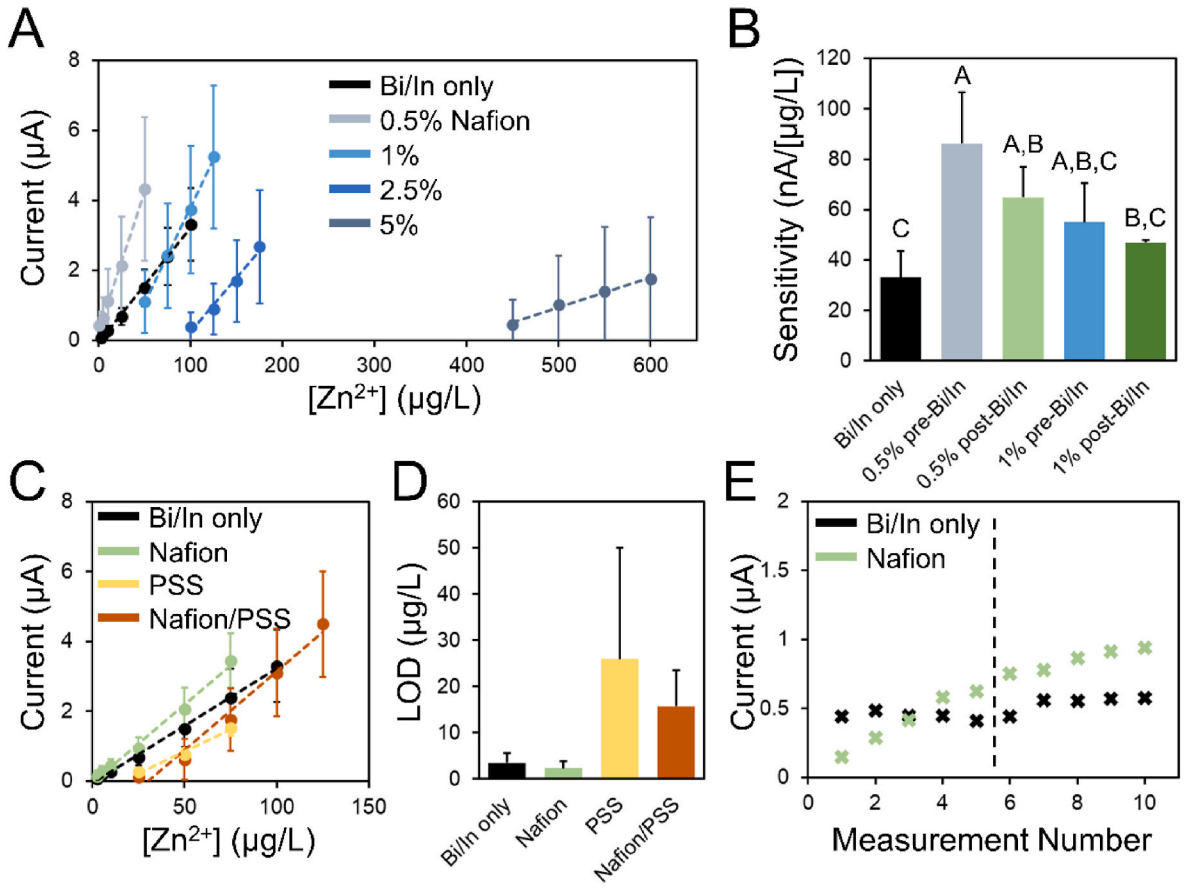

Fig. 3. (A) Calibration curves for Zn^{2+} detection using GCE coated with Nafion pre-Bi/In deposition showed improved sensor performance with decreasing Nafion concentrations. (B) Nafion (0.5%) significantly improves the sensitivity of Bi/In-GCEs and adding the Nafion coating post-Bi/In deposition reduces variability between sensors. LODs were statistically similar, and averages ranged from 3.5 to 15.6 μg/L Zn^{2+}. (C) Calibration curves for Zn^{2+} detection using Bi/In-GCE modified with different charge-selective polymers indicated Nafion improved the sensitivity. (D) Nafion reduced the LOD to Zn^{2+} whereas the addition of PSS increased the LOD. (E) Repeatability over 10 consecutive measurements in KRB containing 50 μg/L Zn^{2+} is shown for a representative Nafion-Bi/In-GCE compared to Bi/In-GCE. Error bars represent standard deviation (n = 3 A,B; n = 5 C,D, and Bi/In only). Letters indicate statistically different groups based on one-way ANOVA with Tukey-Kramer multiple comparison test; $p < 0.05$.

To determine whether Nafion was best suited for the sensor application, we compared the performance of the Nafion-Bi/In-GCE to other charge-selective polymers reported previously, including PSS (Ma et al., 2020) and Nafion/PSS (Jia et al., 2007; Rocha et al., 2006) (n = 5). PSS represents a well-established cation-exchange polymer that improves the stability and reproducibility of Bi-film electrodes (Jia et al., 2007). Shown in Fig. 3C and D, coatings that included PSS (i.e., PSS-Bi/In-GCE and Nafion/PSS-Bi/In-GCE) produced highly variable sensors with sensitivity values of 25.1 ± 4.9 and 45 ± 11.5 nA/(μg/L Zn^{2+}) and LODs of 26.0 ± 24.1 and 15.7 ± 7.8 μg/L Zn^{2+}, respectively, which did not encompass the target Zn^{2+} concentrations (0.45–6 μg/L). Therefore, the Nafion-Bi/In-GCE configuration was ultimately selected for application to Zn^{2+} detection from β-cells, with a sensitivity of 44.7 ± 10.8 nA/(μg/L Zn^{2+}) and low LOD of 2.3 ± 1.5 μg/L Zn^{2+}. To assess the stability of the sensor over multiple ASV cycles, repeated measurements were performed on standard solutions (50 μg/L Zn^{2+} in KRB) using Bi/In-GCEs with and without Nafion (Fig. 3E). The Bi/In-GCE exhibited high reproducibility over 10 consecutive measurements (RSD = 11.9 ± 1.0%, n = 3), consistent with previous studies of Bi-modified electrodes (Wang et al., 2000). The Nafion-Bi/In-GCE, on the other hand, exhibited

a current signal that increased modestly with ASV cycle number prior to stabilizing after roughly 6 cycles ($RSD_{6\text{-}10} = 11.6 \pm 2.9\%$, n = 2). Such transient signal increases have been previously attributed to the partial trapping of oxidized Zn^{2+} ions within pores of the Nafion polymer, subsequently facilitating their deposition (Kefala et al., 2004). To avoid these initial electrode instability effects, all sensors were equilibrated and used to generate calibration curves prior to use for unknown sample measurements. Such an approach ensured that sample measurements were made using a stabilized sensor.

As summarized in Table 1, the sensor performance of the Nafion-Bi/In-GCE was largely comparable to other recently reported electrochemical Zn^{2+} sensors based on modified carbon electrodes, with most studies using acetate buffer as the detection medium. The Nafion-Bi/In-GCE exhibited a sensitivity of 417.3 ± 124.3 nA/(μg/L Zn^{2+}) in sodium acetate buffer (pH 4.3), which was roughly 10 times greater than values obtained in KRB (n = 3 and 5 respectively, Fig. S2). The reduced sensor sensitivity in KRB is likely owing to a number of factors, including i) the increase in free Zn^{2+} ions at lower pH values (Borrill et al., 2019), ii) relatively high concentrations of other salts present in KRB, and iii) sequestration of Zn^{2+} by BSA in KRB (Lu et al., 2008). Such results further highlight the challenge of detecting Zn^{2+} at neutral pH in more complex, physiological solutions.

3.3. Electrochemical and morphological characterization of modified GCEs

To determine how surface modifications altered electrode morphology, SEM analyses were conducted (Fig. 4A). Bare GCEs exhibited a highly uniform surface devoid of any large features, with only minor scratches leftover from polishing. In contrast, Bi/In-GCEs displayed a rough surface, consisting of bright, dispersed clusters, consistent with published morphological studies (Švancara et al., 2005; Vladislavić et al., 2016). For Nafion-Bi/In-GCEs, the Bi/In deposits were covered by the Nafion coating, which appeared as a smooth layer. Interestingly, at higher magnifications, small pores and cracks were observed in the Nafion polymer, which have been attributed to solvent evaporation (Kefala et al., 2004).

The modified GCEs were also characterized electrochemically using a standard redox couple (5 mM $[Fe(CN)]^{3-/4-}$ in 1 M KCl). CV was performed to compare the effect of GCE modifications on oxidation-reduction reactions occurring at the electrode (Fig. 4B). The peak current of the Bi/In-GCE CV was increased relative to the bare GCE curve, indicating that Bi/In facilitated charge transfer by increasing the active surface area. Conversely, the Nafion-GCE and Nafion-Bi/In-GCE CVs exhibited considerably depressed peaks due to charge interactions between negatively charged pores in the Nafion polymer and $[Fe(CN)]^{3-}$ ions, resulting in blocked charge transfer.

EIS was performed to further characterize electron transfer kinetics in the modified GCE. Bi/In-GCEs displayed favorable charge transfer properties, as shown in the Bode plot (Fig. 4C) by lower impedance values and phase angles around −45° in the low-frequency range, which is indicative of increased electron permeability (Laschuk et al., 2021). In contrast, GCEs coated with Nafion showed decreased charge transfer to $[Fe(CN)]^{3-}$, exhibiting higher impedances in both the Bode and Nyquist plots (Fig. 4C and D) and phase angles near the maximum of −90°, consistent with an insulating layer (Laschuk et al., 2021).

3.4. Detection of Zn^{2+} secreted from glucose-stimulated pancreatic β-cells

To encompass the full range of Zn^{2+} concentrations estimated to be secreted by β-cells (0.45–6 μg/L), the effect of pre-concentration time was interrogated as a strategy to expand the dynamic range of the sensor. The 6-min pre-concentration time used for developing the Nafion-Bi/In-GCE sensor configuration provided a linear range of 2.5–500 μg/L Zn^{2+} (Fig. 5A and Fig. S3), which only captured the upper bounds of the target concentration range. By increasing pre-concentration time, lower Zn^{2+} concentrations (e.g., 1 μg/L) were more easily detected (Fig. 5B and C). Interestingly, longer (10 min) pre-

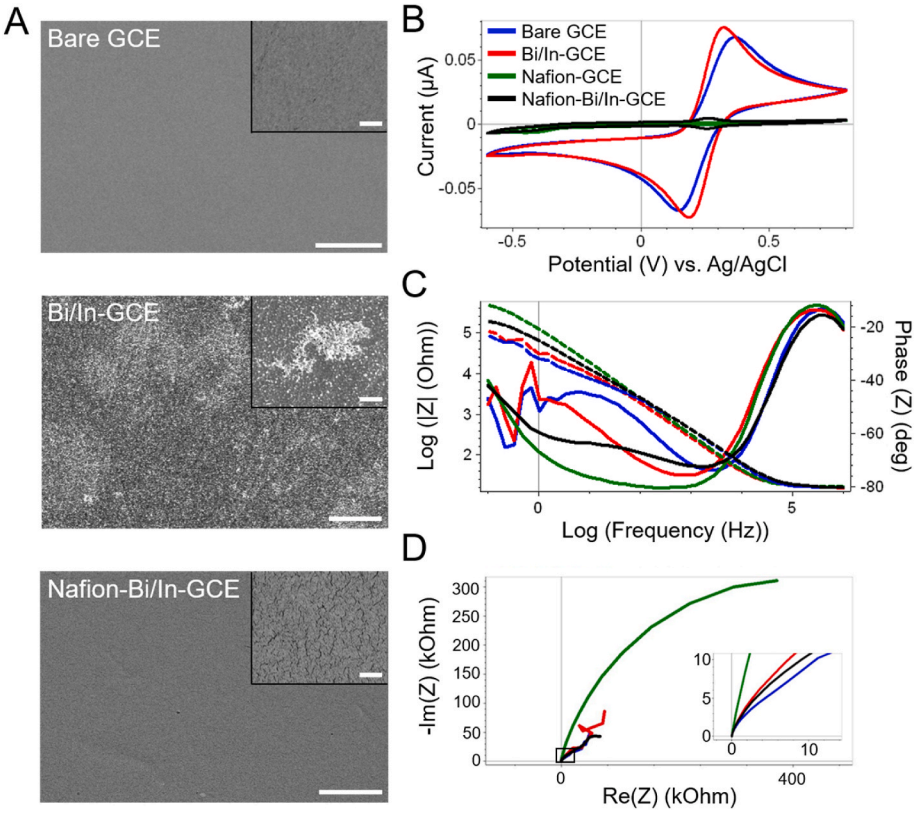

Fig. 4. (A) SEM micrographs of the electrode surface for Bare GCE, Bi/In-GCE, and Nafion-Bi/In-GCE. Scale bar = 5 μm (inset: 500 nm). (B) Representative CV plots of GCE with different modifications in a 5 mM $[Fe(CN)]^{3-/4-}$ (1 M KCl) solution at 50 mV/s show that Nafion blocks negatively charged molecules from reaching the electrode surface. (C) Representative Bode plots of GCE with different modifications plot the impedance (Z) (*dashed lines*) and phase (*solid lines*) against the frequency. (D) Representative Nyquist plots of GCE with different modifications feature real and imaginary components of the impedance (Z).

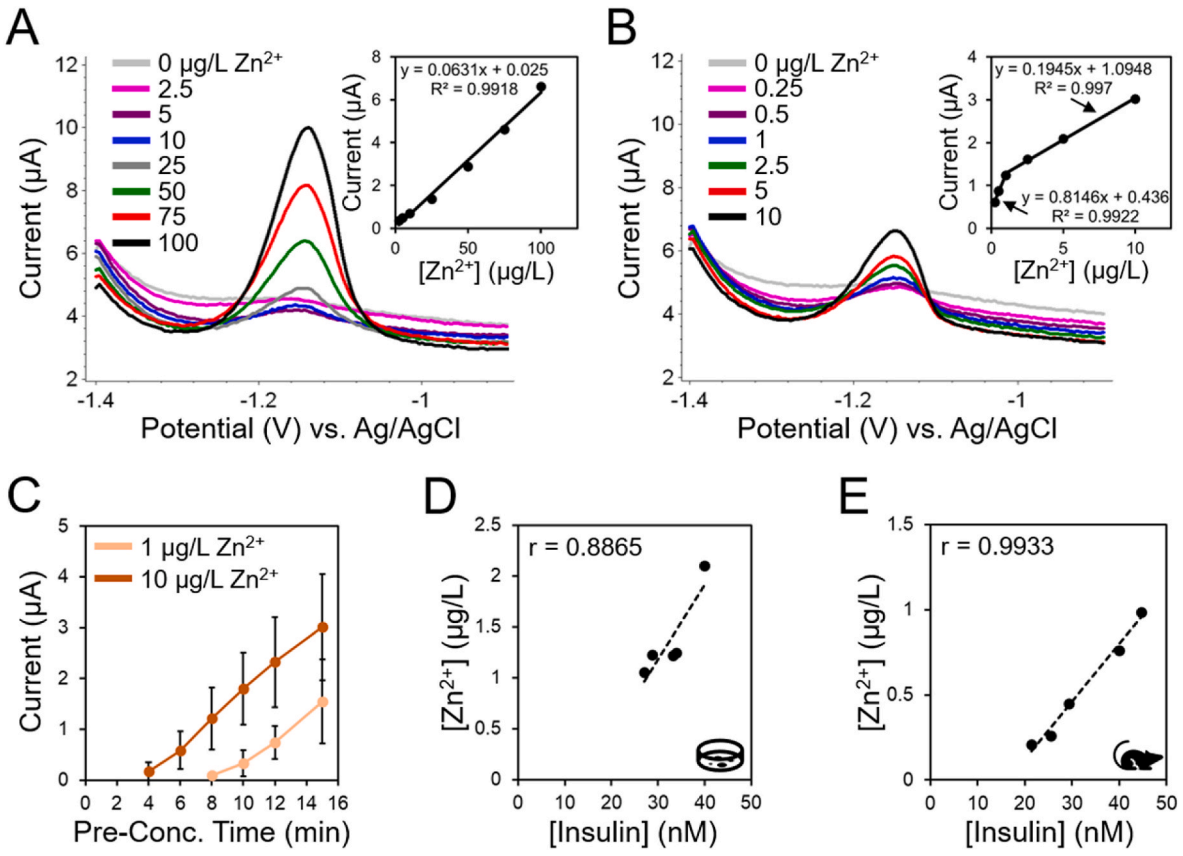

Fig. 5. Representative plots showing ASV curves for increasing concentrations of Zn^{2+} and corresponding calibration curve (inset) for Nafion-Bi/In-GCEs using a pre-concentration time of (A) 6 min and (B) 10 min. Increasing the pre-concentration time enables detection of sub-µg/L concentrations of Zn^{2+}. (C) Effect of pre-concentration time on peak height for two concentrations of Zn^{2+}. Error bars represent standard deviation (n = 3). Correlation between Zn^{2+} measured by ASV and insulin measured by ELISA secreted from glucose-stimulated (D) INS-1 β-cells and (E) mouse islets. The correlation coefficient (r) is displayed on each graph.

concentration periods produced calibration curves with two distinct linear regions of 0.25–1 and 1–10 µg/L Zn^{2+} (Fig. 5B). Several examples of bilinear responses have been reported (Lee et al., 2016; Ruslan et al., 2017; Zhang et al., 2019), and may be related to transport kinetics through porous layers (i.e., Nafion) (Zeinu et al., 2016). Compared to 6-min pre-concentration results, applying the longer 10-min pre-concentration yielded further improved LODs of 0.18 ± 0.12 µg/L Zn^{2+} and higher sensitivities of 203.4 ± 32.9 nA/(µg/L Zn^{2+}) and 1022.6 ± 334.4 nA/(µg/L Zn^{2+}) in the upper and lower linear regions, respectively (n = 5). Importantly, the ASV peak for Zn^{2+} appeared at −1.15 V (Fig. 5A and B), which was consistent with previously reported studies (Kefala et al., 2004; Ouyang et al., 2018) and demonstrated the selectivity and specificity of the sensor.

The application of the Nafion-Bi/In-GCE sensor to Zn^{2+} detection from glucose-stimulated β-cells was validated in two β-cell populations under controlled and isolated conditions ex vivo. INS-1 rat insulinoma cells, an established β-cell line exhibiting robust GSIS (Hohmeier et al., 2000), provided large sample volumes for initial validation testing. In the high glucose (15 mM) samples, the amount of Zn^{2+} detected by the Nafion-Bi/In-GCE correlated well with the insulin concentration as measured by standard ELISAs (r = 0.8865, n = 5), as shown in Fig. 5D. To further confirm sensor compatibility with a more physiologically relevant β-cell source, the experiment was repeated with freshly isolated mouse islets. Indeed, the Zn^{2+} and insulin detected in the high glucose (28 mM) samples were highly correlated (r = 0.9933, n = 5), supporting our hypothesis that Zn^{2+} can be measured as an indirect indicator of insulin secretion from β-cells (Fig. 5E). Together, the amount of secreted insulin and Zn^{2+} were detected from INS-1 cells and mouse islets at an average molar ratio of 3.2, approaching the theoretical ratio of 6 insulin molecules complexed with 2 Zn^{2+} ions present in insulin granules (Fu et al., 2013b). Deviations from theoretical amounts in individual samples could be caused by unregulated diffusion of cytosolic Zn^{2+} into the supernatant or nonspecific binding of secreted Zn^{2+} ions in the buffer solution. A major advantage of this Zn^{2+} sensing approach is the substantially shorter experimental time relative to insulin ELISA protocols, approximately 10 min compared to 3 h, respectively. Furthermore, this approach is more cost-effective than conventional immunoassays since Nafion-Bi/In-GCEs can be polished and reused, in contrast to single-use ELISAs.

4. Conclusion

In summary, we have developed a highly sensitive electrochemical Zn^{2+} sensor for ASV using GCEs modified with Bi/In and coated with the charge-selective polymer Nafion. The electrodeposited Bi/In film effectively improved GCE charge transfer properties, resulting in low LODs, high sensitivity to Zn^{2+}, and wide detection ranges. Compared to other published Zn^{2+} sensors, a similar or improved sensitivity and LOD was achieved presently in a more complex biological medium environment representing physiological pH as well as ionic composition and strength. Furthermore, we demonstrated feasibility in the target application of detecting Zn^{2+} secreted from pancreatic β-cells in correlation with the glucose-stimulated insulin response, as detected using a standard insulin ELISA. However, within the constraints of the experimental set-up used in this initial study, the low-glucose (2.8 mM) samples produced ASV peaks below the linear dynamic range of the Zn^{2+} sensor, a limitation that suggests further development may be needed to detect basal secretion levels. Given the overall goal of measuring dynamic β-cell function in situ, future studies will focus on modifying and scaling the Nafion-Bi/In-GCE for integration into a microfluidic lab-on-a-chip

for real-time detection of glucose-stimulated Zn^{2+} secretion.

CRediT authorship contribution statement

Emma L. Vanderlaan: Conceptualization, Investigation, Visualization, Writing – original draft. **James K. Nolan:** Conceptualization, Investigation, Visualization, Writing – review & editing. **Joshua Sexton:** Investigation, Writing – review & editing. **Carmella Evans-Molina:** Writing – review & editing, Supervision. **Hyowon Lee:** Conceptualization, Writing – review & editing, Supervision. **Sherry L. Voytik-Harbin:** Conceptualization, Writing – original draft, Supervision.

Declaration of competing interest

The authors declare that they have no known competing financial interests or personal relationships that could have appeared to influence the work reported in this paper.

Data availability

Data will be made available on request.

Acknowledgements

This work was supported by generous donations from the McKinley Family Foundation and by the National Science Foundation (United States) under the grant ECCS-1944480. This publication was made possible with fellowship support from Grant Number, UL1TR002529 (S. Moe and S. Wiehe, co-PIs) from the National Institutes of Health (NIH), National Center for Advancing Translational Sciences, Clinical and Translational Sciences Award and Grant Number, 2T32DK101001 (S. Voytik-Harbin, PI) from the NIH, National Institute of Diabetes and Digestive and Kidney Diseases. Additionally, core services were provided by the Islet and Physiology Core in the Indiana Diabetes Research Center (NIH P30 DK097512) and the Life Science Microscopy Facility at Purdue University.

Appendix A. Supplementary data

Supplementary data to this article can be found online at https://doi.org/10.1016/j.bios.2023.115409.

References

Adewola, A.F., Lee, D., Harvat, T., Mohammed, J., Eddington, D.T., Oberholzer, J., Wang, Y., 2010. Biomed. Microdevices 12 (3), 409–417.
Akhavan, O., Ghaderi, E., Rahighi, R., 2012. ACS Nano 6 (4), 2904–2916.
Alcazar, O., Buchwald, P., 2019. Front. Endocrinol. 10, 680.
Bansod, B., Kumar, T., Thakur, R., Rana, S., Singh, I., 2017. Biosens. Bioelectron. 94, 443–455.
Bauer, S., Wennberg Huldt, C., Kanebratt, K.P., Durieux, I., Gunne, D., Andersson, S., Ewart, L., Haynes, W.G., Maschmeyer, I., Winter, A., Ammala, C., Marx, U., Andersson, T.B., 2017. Sci. Rep. 7 (1), 14620.
Borrill, A.J., Reily, N.E., Macpherson, J.V., 2019. Analyst 144 (23), 6834–6849.
Brown, R.J., Milton, M.J., 2005. TrAC, Trends Anal. Chem. 24 (3), 266–274.
Centers for Disease Control and Prevention, 2022. National Diabetes Statistics Report. Centers for Disease Control and Prevention, U.S. Dept of Health and Human Services, Atlanta, GA, 2022.
Chaiyo, S., Mehmeti, E., Žagar, K., Siangproh, W., Chailapakul, O., Kalcher, K., 2016. Anal. Chim. Acta 918, 26–34.
Chen, C., Xie, Q., Yang, D., Xiao, H., Fu, Y., Tan, Y., Yao, S., 2013. RSC Adv. 3 (14), 4473–4491.
Chen, S., Huang, Z., Kidd, H., Kim, M., Suh, E.H., Xie, S., Ghazvini Zadeh, E.H., Xu, Y., Sherry, A.D., Scherer, P.E., Li, W.-H., 2021. Front. Endocrinol. 12, 613964-613964.
Davidson, H.W., Wenzlau, J.M., O'Brien, R.M., 2014. Trends Endocrinol. Metabol. 25 (8), 415–424.
DiMeglio, L.A., Evans-Molina, C., Oram, R.A., 2018. Lancet 391 (10138), 2449–2462.
Dishinger, J.F., Reid, K.R., Kennedy, R.T., 2009. Anal. Chem. 81 (8), 3119–3127.
Easley, C.J., Rocheleau, J.V., Head, W.S., Piston, D.W., 2009. Anal. Chem. 81 (21), 9086–9095.
Economou, A., 2005. TrAC, Trends Anal. Chem. 24 (4), 334–340.
Eizirik, D.L., Pasquali, L., Cnop, M., 2020. Nat. Rev. Endocrinol. 16 (7), 349–362.
Fonseca, W.T., Takeuchi, R.M., Santos, A.L., 2015. Electroanalysis 27 (7), 1616–1624.
Fu, L., Li, X., Yu, J., Ye, J., 2013a. Electroanalysis 25 (2), 567–572.
Fu, Z., Gilbert, E.R., Liu, D., 2013b. Curr. Diabetes Rev. 9 (1), 25–53.
Gamble, A., Pepper, A.R., Bruni, A., Shapiro, A.M.J., 2018. Islets 10 (2), 80–94.
Ghazvini Zadeh, E.H., Huang, Z., Xia, J., Li, D., Davidson, H.W., Li, W.-H., 2020. Cell Rep. 32 (2), 107904.
Glieberman, A.L., Pope, B.D., Zimmerman, J.F., Liu, Q., Ferrier, J.P., Kenty, J.H.R., Schrell, A.M., Mukhitov, N., Shores, K.L., Tepole, A.B., Melton, D.A., Roper, M.G., Parker, K.K., 2019. Lab Chip 19 (18), 2993–3010.
Gudić, S., Smoljko, I., Kliškić, M., 2010. J. Alloys Compd. 505 (1), 54–63.
Hasslacher, C., Kulozik, F., Platten, I., 2014. J. Diabetes Sci. Technol. 8 (3), 466–472.
Henquin, J.-C., 2021. Mol. Metabol. 48, 101212.
Hering, B.J., Clarke, W.R., Bridges, N.D., Eggerman, T.L., Alejandro, R., Bellin, M.D., Chaloner, K., Czarniecki, C.W., Goldstein, J.S., Hunsicker, L.G., Kaufman, D.B., Korsgren, O., Larsen, C.P., Luo, X., Markmann, J.F., Naji, A., Oberholzer, J., Posselt, A.M., Rickels, M.R., Ricordi, C., Robien, M.A., Senior, P.A., Shapiro, A.M., Stock, P.G., Turgeon, N.A., 2016. Diabetes Care 39 (7), 1230–1240.
Hohmeier, H.E., Mulder, H., Chen, G., Henkel-Rieger, R., Prentki, M., Newgard, C.B., 2000. Diabetes 49 (3), 424–430.
Integrated Islet Distribution Program, 2020. Potency Test: Glucose Stimulated Insulin Release Assay. protocols.Io dx.doi.org/10.17504/protocols.io.Bhdqj25w.
Jia, J., Cao, L., Wang, Z., 2007. Electroanalysis 19 (17), 1845–1849.
Jun, Y., Lee, J., Choi, S., Yang, J.H., Sander, M., Chung, S., Lee, S.H., 2019. Sci. Adv. 5 (11), eaax4520.
Kefala, G., Economou, A., Voulgaropoulos, A., 2004. Analyst 129 (11), 1082–1090.
Kefala, G., Economou, A., Voulgaropoulos, A., Sofoniou, M., 2003. Talanta 61 (5), 603–610.
Kim, J., de Araujo, W.R., Samek, I.A., Bandodkar, A.J., Jia, W., Brunetti, B., Paixão, T.R. L.C., Wang, J., 2015. Electrochem. Commun. 51, 41–45.
Kokab, T., Shah, A., Iftikhar, F.J., Nisar, J., Akhter, M.S., Khan, S.B., 2019. ACS Omega 4 (26), 22057–22068.
Kratz, S.R.A., Höll, G., Schuller, P., Ertl, P., Rothbauer, M., 2019. Biosensors 9 (3), 110.
Kudr, J., Richtera, L., Nejdl, L., Xhaxhiu, K., Vitek, P., Rutkay-Nedecky, B., Hynek, D., Kopel, P., Adam, V., Kizek, R., 2016. Materials 9 (1), 31.
Laschuk, N.O., Easton, E.B., Zenkina, O.V., 2021. RSC Adv. 11 (45), 27925–27936.
Lee, S., Bong, S., Ha, J., Kwak, M., Park, S.-K., Piao, Y., 2015. Sensor. Actuator. B Chem. 215, 62–69.
Lee, S., Oh, J., Kim, D., Piao, Y., 2016. Talanta 160, 528–536.
Li, D., Chen, S., Bellomo, E.A., Tarasov, A.I., Kaut, C., Rutter, G.A., Li, W.H., 2011. Proc. Natl. Acad. Sci. U. S. A 108 (52), 21063–21068.
Li, S., Zhang, C., Wang, S., Liu, Q., Feng, H., Ma, X., Guo, J., 2018. Analyst 143 (18), 4230–4246.
Lomasney, A.R., Yi, L., Roper, M.G., 2013. Anal. Chem. 85 (16), 7919–7925.
Lu, J., Stewart, A.J., Sadler, P.J., Pinheiro, T.J., Blindauer, C.A., 2008. Biochem. Soc. Trans. 36 (6), 1317–1321.
Lu, Z., Zhang, J., Dai, W., Lin, X., Ye, J., Ye, J., 2017. Microchim. Acta 184 (12), 4731–4740.
Ma, S., Wei, H., Pan, D., Pan, F., Wang, C., Kang, Q., 2020. J. Electrochem. Soc. 167 (4), 046519.
Maghasi, A.T., Halsall, H.B., Heineman, W.R., Rodriguez Rilo, H.L., 2004. Anal. Biochem. 326 (2), 183–189.
Martínez-Periñán, E., Revenga-Parra, M., Gennari, M., Pariente, F., Mas-Ballesté, R., Zamora, F., Lorenzo, E., 2016. Sensor. Actuator. B Chem. 222, 331–338.
Misun, P.M., Yesildag, B., Forschler, F., Neelakandhan, A., Rousset, N., Biernath, A., Hierlemann, A., Frey, O., 2020. Adv. Biosyst. 4 (3), 1900291.
Nathan, D.M., 2014. DCCT/Edic research group. Diabetes Care 37 (1), 9–16.
Ouyang, R., Xu, L., Wen, H., Cao, P., Jia, P., Lei, T., Zhou, X., Tie, M., Fu, X., Zhao, Y., Chang, H., Miao, Y., 2018. Int. J. Electrochem. Sci. 13, 1423–1440.
Patel, S., Ishahak, M., Chaimov, D., Velraj, A., LaShoto, D., Hagan, D., Buchwald, P., Phelps, E., Agarwal, A., Stabler, C., 2021. Sci. Adv. 7 (7) eaba5515.
Pettus, J.H., Zhou, F.L., Shepherd, L., Preblick, R., Hunt, P.R., Paranjape, S., Miller, K.M., Edelman, S.V., 2019. Diabetes Care 42 (12), 2220–2227.
Qian, W.-J., Gee, K.R., Kennedy, R.T., 2003. Anal. Chem. 75 (14), 3468–3475.
Qian, W.-J., Peters, J.L., Dahlgren, G.M., Gee, K.R., Kennedy, R.T., 2004. Biotechniques 37 (6), 922–933.
Ren, W., Zhang, Y., Li, M., 2018. Int. J. Electrochem. Sci. 13, 1331–1342.
Rocha, L.S., Pinheiro, J.P., Carapuça, H.M., 2006. Langmuir 22 (19), 8241–8247.
Romih, T., Hočevar, S.B., Kononenko, V., Drobne, D., 2017. Sensor. Actuator. B Chem. 238, 1277–1282.
Ruslan, N.I., Lim, D.C.K., Alang Ahmad, S.A., Abdul Aziz, S.F.N., Supian, F.L., Yusof, N. A., 2017. J. Electroanal. Chem. 799, 497–504.
Sakthivel, R., Prasanna, S.B., Tseng, C.L., Lin, L.Y., Duann, Y.F., He, J.H., Chung, R.J., 2022. Small 18 (35), 2202516.
Schulze, T., Mattern, K., Erfle, P., Brüning, D., Scherneck, S., Dietzel, A., Rustenbeck, I., 2021. Front. Bioeng. Biotechnol. 9 (158), 615639.
Serrano, N., Alberich, A., Díaz-Cruz, J.M., Ariño, C., Esteban, M., 2013. TrAC, Trends Anal. Chem. 46, 15–29.
Shrivastava, A., Gupta, V.B., 2011. Chronicles Young Sci. 2 (1), 21–25.
Šišoláková, I., Hovancová, J., Oriňaková, R., Oriňak, A., Trnková, L., García, D.R., Radoňak, J., 2019. Bioelectrochemistry 130, 107326.
Soffe, R., Nock, V., Chase, J.G., 2019. ACS Sens. 4 (1), 3–19.
Švancara, I., Baldrianova, L., Vlcek, M., Metelka, R., Vytras, K., 2005. Electroanalysis 17 (2), 120–126.
Švancara, I., Prior, C., Hočevar, S.B., Wang, J., 2010. Electroanalysis 22 (13), 1405–1420.

Trachioti, M.G., Hrbac, J., Prodromidis, M.I., 2018. Sensor. Actuator. B Chem. 260, 1076–1083.
Velazco-Cruz, L., Song, J., Maxwell, K.G., Goedegebuure, M.M., Augsornworawat, P., Hogrebe, N.J., Millman, J.R., 2019. Stem Cell Rep. 12 (2), 351–365.
Vladislavić, N., Buzuk, M., Brinić, S., Buljac, M., Bralić, M., 2016. J. Solid State Electrochem. 20 (8), 2241–2250.
Wang, J., 2005. Electroanalysis 17 (15-16), 1341–1346.
Wang, J., Lu, J., Hocevar, S.B., Farias, P.A., Ogorevc, B., 2000. Anal. Chem. 72 (14), 3218–3222.
Wang, J., Lu, J., Kirgöz, Ü.A., Hocevar, S.B., Ogorevc, B., 2001. Anal. Chim. Acta 434 (1), 29–34.
Witkowski, P., Philipson, L.H., Kaufman, D.B., Ratner, L.E., Abouljoud, M.S., Bellin, M. D., Buse, J.B., Kandeel, F., Stock, P.G., Mulligan, D.C., 2021. Am. J. Transplant. 21 (4), 1365–1375.
Wu, W., Jia, M., Wang, Z., Zhang, W., Zhang, Q., Liu, G., Zhang, Z., Li, P., 2019. Microchim. Acta 186 (2), 1–10.
Xing, Y., Nourmohammadzadeh, M., Elias, J.E., Chan, M., Chen, Z., McGarrigle, J.J., Oberholzer, J., Wang, Y., 2016. Biomed. Microdevices 18 (5), 80.
Xu, M., Luo, X., Davis, J.J., 2013. Biosens. Bioelectron. 39 (1), 21–25.
Xu, Z., Kim, G.-H., Han, S.J., Jou, M.J., Lee, C., Shin, I., Yoon, J., 2009. Tetrahedron 65 (11), 2307–2312.
Zeinu, K.M., Hou, H., Liu, B., Yuan, X., Huang, L., Zhu, X., Hu, J., Yang, J., Liang, S., Wu, X., 2016. J. Mater. Chem. 4 (36), 13967–13979.
Zhang, Y., Jiang, X., Zhang, J., Zhang, H., Li, Y., 2019. Biosens. Bioelectron. 130, 315–321.